

Probabilistic Evaluation of the Dynamics and Predictability of the Mesoscale Convective Vortex of 10–13 June 2003

DANIEL P. HAWBLITZEL

Department of Atmospheric Sciences, Texas A&M University, College Station, Texas, and National Weather Service, Wilmington, Ohio

FUQING ZHANG AND ZHIYONG MENG

Department of Atmospheric Sciences, Texas A&M University, College Station, Texas

CHRISTOPHER A. DAVIS

National Center for Atmospheric Research, Boulder, Colorado*

(Manuscript received 14 September 2005, in final form 14 July 2006)

ABSTRACT

This study examines the dynamics and predictability of the mesoscale convective vortex (MCV) of 10–13 June 2003 through ensemble forecasting. The MCV of interest developed from a preexisting upper-level disturbance over the southwest United States on 10 June and matured as it traveled northeastward. This event is of particular interest given the anomalously strong and long-lived nature of the circulation. An ensemble of 20 forecasts using a 2-way nested mesoscale model with horizontal grid increments of 30 and 10 km are employed to probabilistically evaluate the dynamics and predictability of the MCV. Ensemble mean and spread as well as correlations between different forecast variables at different forecast times are examined. It is shown that small-amplitude large-scale balanced initial perturbations may result in very large ensemble spread, with individual solutions ranging from a very strong MCV to no MCV at all. Despite similar synoptic-scale conditions, the ensemble MCV forecasts vary greatly depending on intensity and coverage of simulated convection, illustrating the critical role of convection in the development and evolution of this MCV. Correlation analyses reveal the importance of a preexisting disturbance to the eventual development of the MCV. It is also found that convection near the center of the MCV the day after its formation may be an important factor in determining the eventual growth of a surface vortex and that a stronger midlevel vortex is more conducive to convection, especially on the downshear side, consistent with the findings of previous MCV studies.

1. Introduction

The tendency of a midlevel cyclonic circulation to form within the stratiform rain region of a midlatitude mesoscale convective system (MCS) is a well-documented phenomenon (Zhang and Fritsch 1988; Cotton et al. 1989; Menard and Fritsch 1989; Bartels

and Maddox 1991). This feature, referred to as a mesoscale convective vortex (MCV), was first defined in Zhang and Fritsch (1987) and later in Zhang (1992) as “a significant concentration of positive relative vorticity of magnitude at least that of the local Coriolis parameter, eventually leading to the formation of a closed circulation.” Most MCVs are characterized by horizontal scales as large as several hundred kilometers and time scales ranging from hours to days. In extreme cases, MCVs have been linked to extreme rainfall events, such as the Johnstown, Pennsylvania, flood of 1977 (Bosart and Sanders 1981) and the severe south Texas rainfall event of 2002 (Nielsen-Gammon et al. 2005).

Various studies have shown that an MCV can form in

* The National Center for Atmospheric Research is sponsored by the National Science Foundation.

Corresponding author address: Dr. Fuqing Zhang, Department of Atmospheric Sciences, Texas A&M University, College Station, TX 77845-3150.
E-mail: fzhang@tamu.edu

a variety of ways. The development of one MCV within the stratiform rain region of an MCS was attributed to tilting followed by stretching within a region of evaporative and melting cooling by Zhang (1992). This cooling effect was believed "crucial" to the development of a deep column of positive vorticity in a modeling study by Davis and Trier (2002). Using a potential vorticity (PV) approach, several studies (e.g., Thorpe 1985; Haynes and McIntyre 1987; Raymond and Jiang 1990) have shown that latent heat release, typically maximized in the midtroposphere in an MCS, acts to redistribute PV so that a negative PV anomaly and associated anticyclonic circulation exist above the level of maximum heating, and a positive PV anomaly and cyclonic circulation develop below it. Raymond and Jiang (1990) connected the latter PV anomaly to MCVs in a theoretical study that idealized an MCV as having balanced vertical vorticity and potential temperature distributions. The balanced aspect of MCV structure has been suggested by both observational studies (e.g., Bosart and Sanders 1981; Menard and Fritsch 1989; Bartels and Maddox 1991; Davis and Trier 2007) and numerical simulations (e.g., Zhang and Fritsch 1987; Davis and Weisman 1994).

A noteworthy aspect of some MCVs is their ability to focus additional moist convection during subsequent diurnal cycles, which has been shown to generate significant positive feedback onto the vortex (e.g., Jiang and Raymond 1995; Ritchie and Holland 1997; Montgomery and Enagonio 1998; Davis et al. 2002; Trier and Davis 2002). In an analysis of a large MCS, Fritsch et al. (1994) suggested that the development of subsequent convection can cause an MCV to grow upscale and in some cases become larger and longer-lived than its parent MCS. Resulting midlevel heating from such convection can increase the amplitude of an existing PV anomaly if the convection occurs coincidentally, or it can produce a new MCV altogether. If the local Rossby radius is sufficiently small, additional convective heating may intensify the warm core instead of propagating away as gravity waves. In such cases, the balanced response results in lowered heights beneath the warm anomaly, where PV increases (Raymond and Jiang 1990). In extreme cases, this mechanism allows the vortex to penetrate into the surface cold pool that typically characterizes an MCV. A resulting balanced cyclonic circulation and convergence can then develop or intensify at the surface. Though uncommon, this convectively enhanced surface convergence can further enhance convection and in turn lengthen the lifetime of an MCV (e.g., Rogers and Fritsch 2001).

The sensitivity of an MCV life cycle to stochastic convective processes has serious impacts on predictabil-

ity. Zhang et al. (2002, 2003, 2006b) and Zhang (2005) demonstrated that small-scale error in the presence of moist convection can significantly impact mesoscale predictability because of strong upscale error growth, similar to that foreseen by Lorenz (1969). Because of the intrinsic uncertainty in initializing and predicting moist convection, Buizza and Chessa (2002) note the significance of including stochastic perturbations in the global ensemble prediction system at the European Centre for Medium-Range Weather Forecasts. Similar studies have documented how prediction skill can be significantly improved when data assimilation techniques account for uncertainties in initial conditions, including the specifications of background error covariance (e.g., Cohn and Parrish 1991; Daley 1992; Evensen 1994; Cohn 1997; Talagrand 1997). Ensemble forecasting, which accounts for initial condition uncertainties and/or model error, was introduced as a considerable step in improving the state of numerical weather prediction (Tracton and Kalnay 1993; Molteni et al. 1996; Toth and Kalnay 1997). Ensemble forecasting not only promises the best estimate of the future atmospheric state, but it also details uncertainties associated with the best estimate and provides valuable information for estimating the flow-dependent background error covariance that is essential for data assimilation (Evensen 1994; Snyder and Zhang 2003; Zhang et al. 2006a).

Zhang (2005) introduced the use of ensemble forecasts to investigate the dynamics and structure of mesoscale error covariance in an extreme extratropical cyclogenesis event. It was demonstrated that underlying balanced dynamics and effects of moist convection determined the characteristics and structure of error growth. The current study seeks to apply this technique to investigate error covariance structure in a small-scale event highly dependent on convective processes, such as an MCV event that occurred on 10–13 June 2003 during the Bow Echo and MCV Experiment (BAMEX; Davis et al. 2004). The 10–13 June MCV spanned more than 60 h and involved three separate episodes of widespread convection, including numerous damaging wind events. The rare long duration of this system and the nature of subsequent convection make it a valuable case study for investigating the role of moist convection in MCV predictability and dynamics.

Understanding the predictability of long-lived MCVs such as the 10–13 June event is important in order to ultimately better comprehend model precipitation forecasts in potential MCV events. Accordingly, this study employs ensemble forecasts in a manner similar to that of Zhang (2005) to evaluate error covariance structure and error growth associated with the long-lived MCV

of 10–13 June 2003 and to provide a better understanding of the dynamics involved in the life cycle of this system. This study also examines the relationship between convective forecasts at all stages of the MCV to the ability to predict the MCV up to 48 h later. To give a more detailed look at this system and its associated convection, an overview of the MCV will be presented in section 2, and a description of the model and experimental design follows in section 3. A probabilistic evaluation of the MCV predictability and dynamics will be discussed in sections 4 and 5, respectively. Concluding remarks can be found in section 6.

2. Case overview

During the period of 5–14 June 2003, a strong subtropical jet (speeds exceeding 50 m s^{-1}) extended from southeast of Hawaii east-northeastward to the Mississippi Valley and North Atlantic, as described in Galarneau and Bosart (2004). A weak upper-level trough, shown in the 300-hPa National Centers for Environmental Prediction Eta analysis at that time (Fig. 1a), was embedded within this strong jet over New Mexico at 0000 UTC 10 June. Ahead of this feature, a large MCS developed over the high plains of eastern New Mexico and southwest Texas between 0000 and 0300 UTC 10 June (Fig. 2a). While the bulk of the west Texas activity moved southward into central Texas by 1200 UTC (Fig. 2b), radar loops showed that a weak cyclonic circulation remained within the stratiform rain region over the central Texas/New Mexico border around 0600 UTC. This feature became evident in the Eta 600-hPa analysis at 1200 UTC 10 June (Fig. 3a). This weak circulation can be traced on radar and satellite loops throughout the day of 10 June as it crossed the Texas Panhandle into western Oklahoma later that evening (Figs. 2a,b show still radar images during this period).

By 0000 UTC 11 June, the 300- and 600-hPa shortwave troughs had translated eastward to western Oklahoma (Figs. 1b, 3b). Significant intensification of the midlevel shortwave is evident through this time (Figs. 3a,b) and is likely the result of superposition of the aforementioned weak cyclonic circulation upon synoptic-scale cyclogenesis. The significance of the disturbance will be discussed later in this paper. Immediately ahead of this feature, an area of convection initiated at 2100 UTC 10 June and by 0000 UTC 11 June had extended from north central Oklahoma through the southwest corner of the state (roughly 250 km in length; see Fig. 2c). An extensive stratiform rain region formed behind the MCS around 0600 UTC (Fig. 2d), and by 0900 UTC 11 June, the MCS had weakened in western

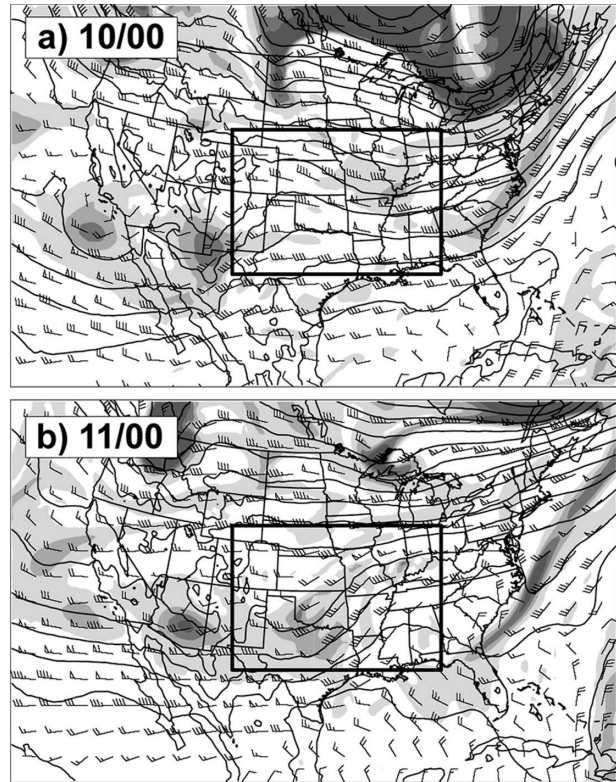


FIG. 1. The 300-hPa Eta analysis of height (every 50 m), wind (full barb 5 m s^{-1}), and PV (shaded every 0.5 PVU) valid at 0000 UTC (a) 10 Jun 2003 and (b) 11 Jun 2003. The box denotes the location of the 10-km nested domain used for this study.

Arkansas while a large area of light-to-moderate rain (roughly 200 km in diameter) remained across eastern Oklahoma and western Arkansas (Fig. 2e). A weak cyclonic circulation within the stratiform region over eastern Oklahoma (denoted by an “L” in Fig. 2d) became evident by 0600 UTC 11 June in radar reflectivity animations and in the 600-hPa Eta analysis (Fig. 3c). The cyclonic circulation grew in strength and size by 1200 UTC 11 June when it was extremely well-defined over northeast Arkansas (Fig. 2f). At this time, 600-hPa heights further lowered at the vortex center (Fig. 3d) and evidence of a closed circulation emerged.

Figures 2g–i show radar reflectivity at 3-h intervals from 1500 UTC 11 June to 0000 UTC 12 June, during which times convection became a significant factor in the evolution of the MCV. This activity is herein referred to as secondary convection, having developed during a diurnal cycle subsequent to the formation of a mature MCV. By 1500 UTC 11 June (Fig. 2g), convection had already restrengthened on the southern periphery of the midlevel circulation, near Little Rock, Arkansas. At the same time, isolated thunderstorms began to develop across a large portion of the southeast

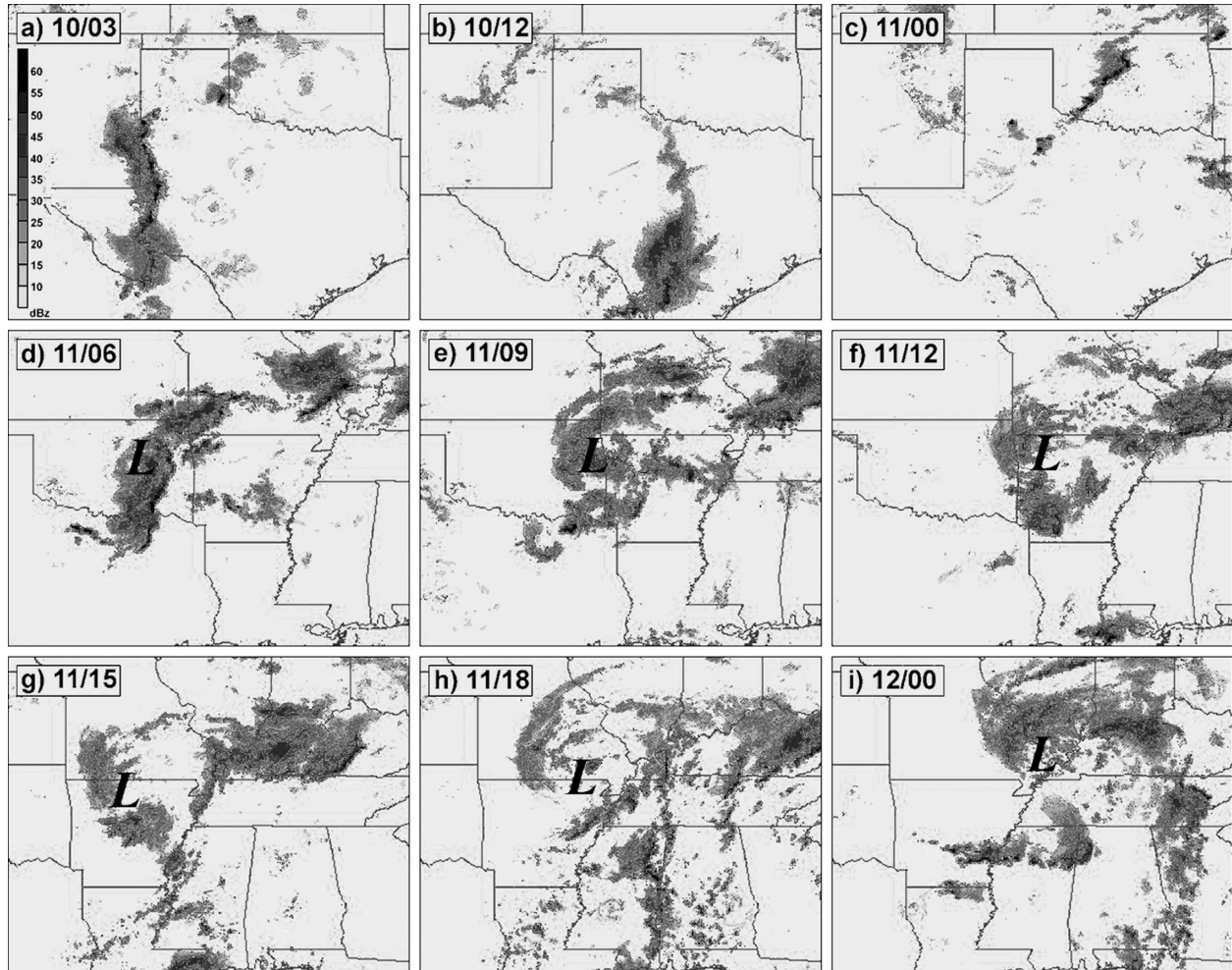


FIG. 2. Radar reflectivity (dBZ) observed at (a) 0300 and (b) 1200 UTC 10 Jun 2003; (c) 0000, (d) 0600, (e) 0900, (f) 1200, (g) 1500, and (h) 1800 UTC 11 Jun 2003; and (i) 0000 UTC 12 Jun 2003. The L denotes the approximate midlevel circulation center for reference.

United States. Closer to the MCV circulation, isolated weak convection initiated around 1800 UTC 11 June in southeast Missouri (Fig. 2h), about 50 km east of the midlevel circulation center. Additional weak convection formed near and slightly west of the MCV circulation through 2100 UTC 11 June (not shown) and expanded throughout the northern flank of the circulation by 0000 UTC 12 June (Fig. 2i). At the surface, a weak surface low of 1006 hPa and a cyclonic circulation appeared in the surface analysis over southwest Missouri at 1200 UTC 11 June (Fig. 4b). The cyclonic circulation broadened by 1800 UTC 11 June (Fig. 4c), around the time that new convection had formed near the MCV center (Fig. 2h). Through 0000 UTC 12 June (Fig. 4d), the surface cyclone intensified and broadened until merging with a nearby frontal boundary. Cross-sectional analyses using both the Eta analyses (Fig. 5) and the BAMEX dropsonde data (not shown) indicate

that the MCV circulation had penetrated deep into the lower troposphere and led to surface low development similar to that in Fritsch et al. (1994) and Rogers and Fritsch (2001). The vortex penetrated the surface cold pool underlying the MCV, though it was displaced roughly 100 km east of the deepest portion of the cold pool.

These observations suggest possible convective enhancement of midlevel vorticity by convection over west Texas early on 10 June, which later resulted in the development of the MCV via the maturity of a large MCS the next evening. Initiation of widespread secondary convection during the local afternoon of 11 June was concurrent with surface cyclogenesis beneath the midlevel MCV. These connections will be explored in detail in section 5 of this study, which will concern the time period from 1200 UTC 10 June to 0000 UTC 12 June, or from the time of a mature MCS over New

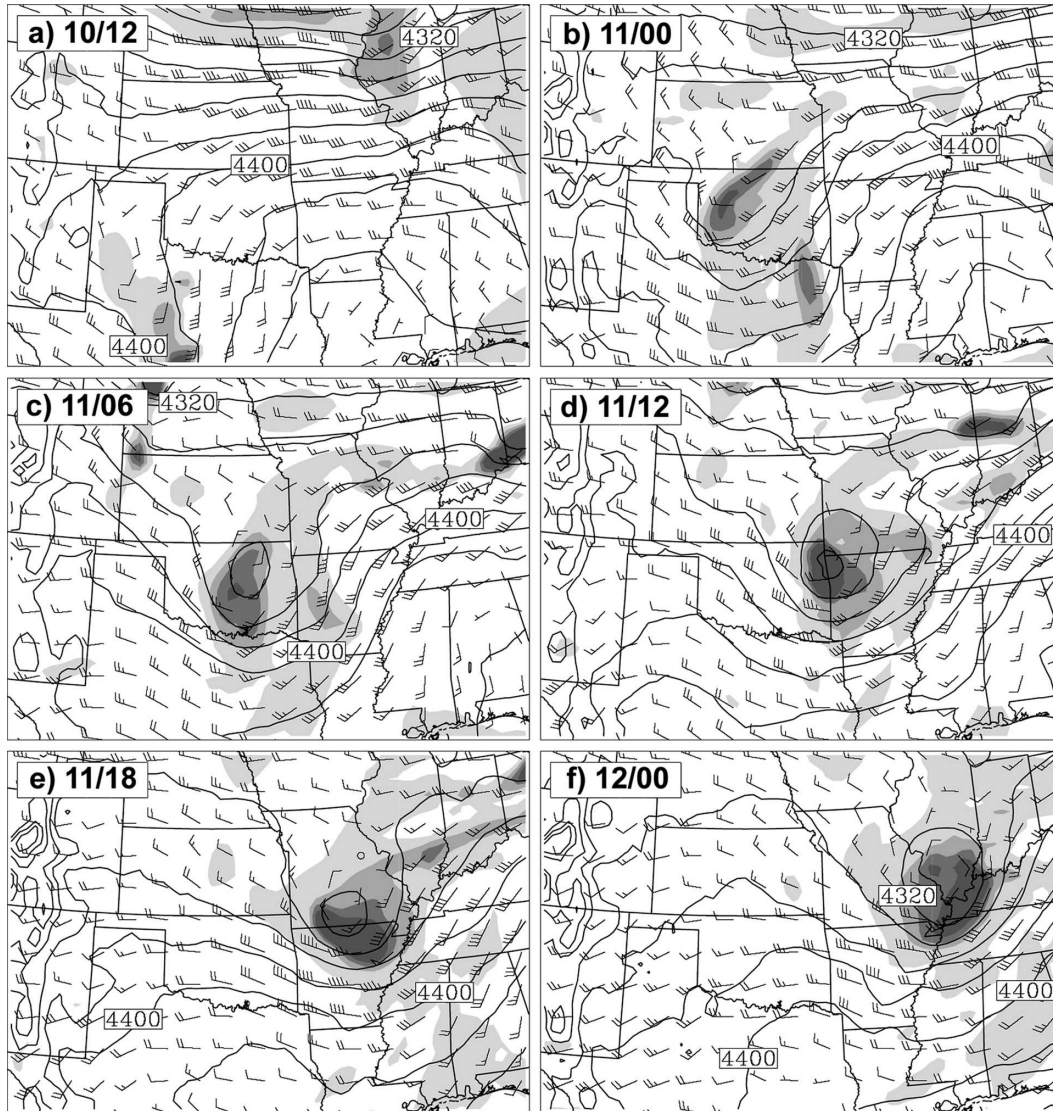


FIG. 3. The 600-hPa Eta analysis of height (every 20 m), wind (full barb 5 m s^{-1}), and PV (shaded every 0.5 PVU) valid at (a) 1200 UTC 10 Jun 2003; (b) 0000, (c) 0600, (d) 1200, and (e) 1800 UTC 11 Jun 2003; and (f) 0000 UTC 12 Jun 2003.

Mexico and western Texas to the development of a mature surface cyclone.

3. Experimental design

a. Forecast model

This study utilizes the two-way nested fifth-generation Pennsylvania State University–National Center for Atmospheric Research (PSU–NCAR) Mesoscale Model (MM5), version 3 (Dudhia 1993). The model is initialized at 0000 UTC 10 June 2003 and integrated for 48 h, using model domains with horizontal grid spacings of 30 and 10 km. The coarse domain uses 190×120 horizontal grid points, which covers the en-

tire continental United States, and the nest domain uses 241×181 grid points (Fig. 1). The fine grid covers the central United States and is meant to capture both the formation and evolution of the MCV. Both domains use 27 layers in a vertically stretched coordinate. The Mellor–Yamada PBL scheme (Mellor and Yamada 1982), the Reisner microphysics scheme with graupel (Reisner et al. 1998), and the Grell cumulus scheme (Grell 1993) are employed for both domains. Simulations use the operational Eta Model analyses (forecasts) as initial (lateral boundary) conditions. The feature of interest is near the center of the coarse grid in order to minimize the impacts of using the same lateral boundary conditions for the coarse grid of all ensemble

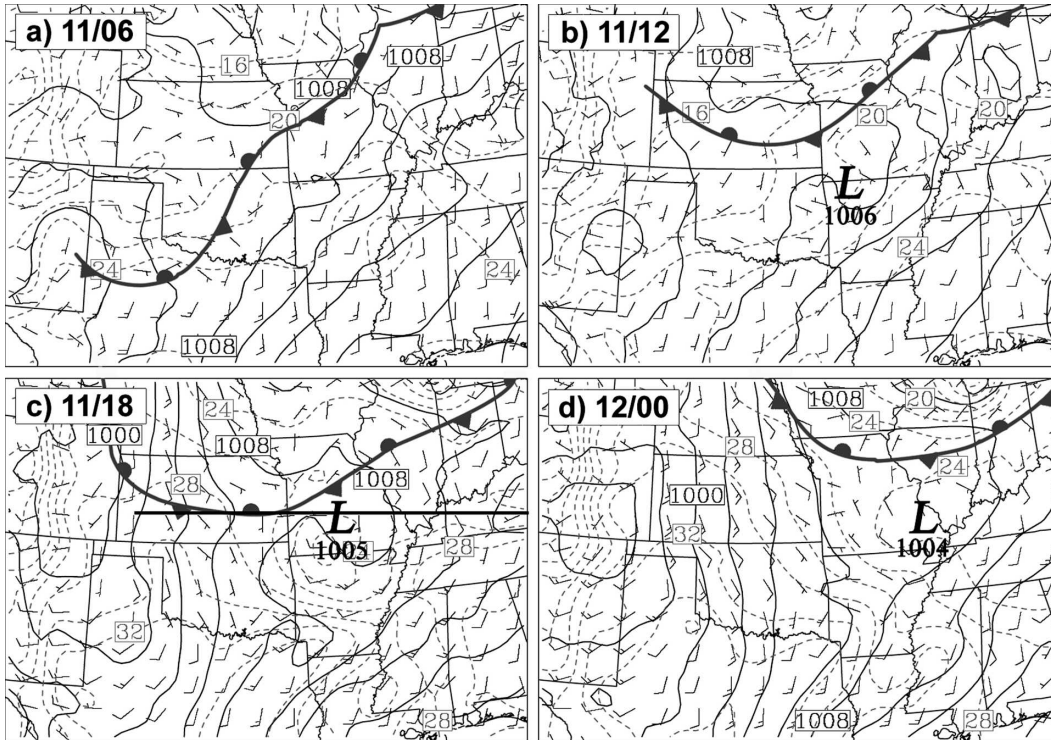


FIG. 4. The Eta analyses of surface temperature (every 2°C), mean sea level pressure (every 2 hPa), and winds (full barb 5 m s⁻¹) valid at (a) 0600, (b) 1200, (c) 1800 UTC 11 Jun 2003; and (d) 0000 UTC 12 Jun 2003. The observed surface low pressure center and a subjective analysis of surface fronts are also depicted.

members. Although high-resolution ensembles are always desirable (but limited by computing resources), a 10-km grid spacing in the current study begins to be “convection permitting” but is distinct from a convection-resolving grid because the individual convective elements are not resolved, yet the organization of convection may be captured to an acceptable degree (Zhang et al. 2007).

b. Ensemble initializations

In a manner similar to Zhang (2005), an ensemble of twenty forecasts is generated using balanced random perturbations. The perturbations are produced by randomly selecting initial perturbations of roughly 1 m s⁻¹ in winds and 0.5 K in temperature from the background error covariance used by the MM5 three-dimensional variational data assimilation (3DVAR) system developed at NCAR (Barker et al. 2004). Twenty sets of random initial streamfunction balanced perturbations are produced and transformed to derive perturbations of wind, temperature, and pressure. These perturbations are added to the reference MM5 analysis at 0000 UTC 10 June to generate 20 ensemble forecasts (numbered EN-01–EN-20; Zhang 2005). Zhang (2005) found that the overall covariance/correlation structure in a

20-member ensemble is qualitatively similar to that of a 40-member ensemble. Therefore, a relatively small ensemble size is used in this study to account for limited computing resources.

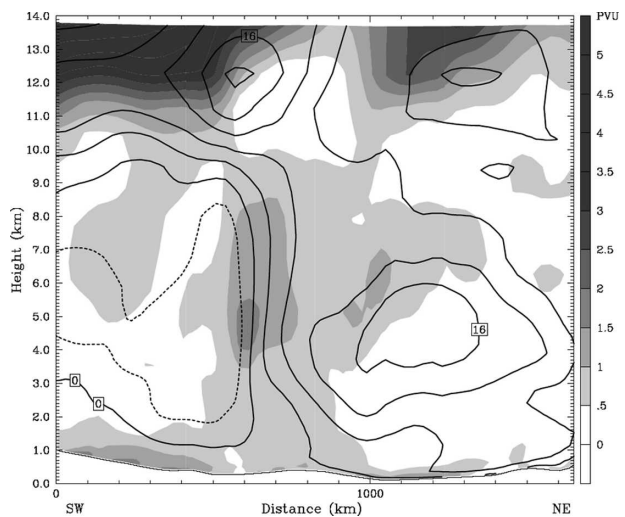


FIG. 5. The Eta vertical cross section analysis of PV (every 0.5 PVU) and the v -component wind (every 4 m s⁻¹; negative, dashed), valid at 1800 UTC 11 Jun 2003. The analysis is taken along the east–west cross section denoted by the black line in Fig. 4c.

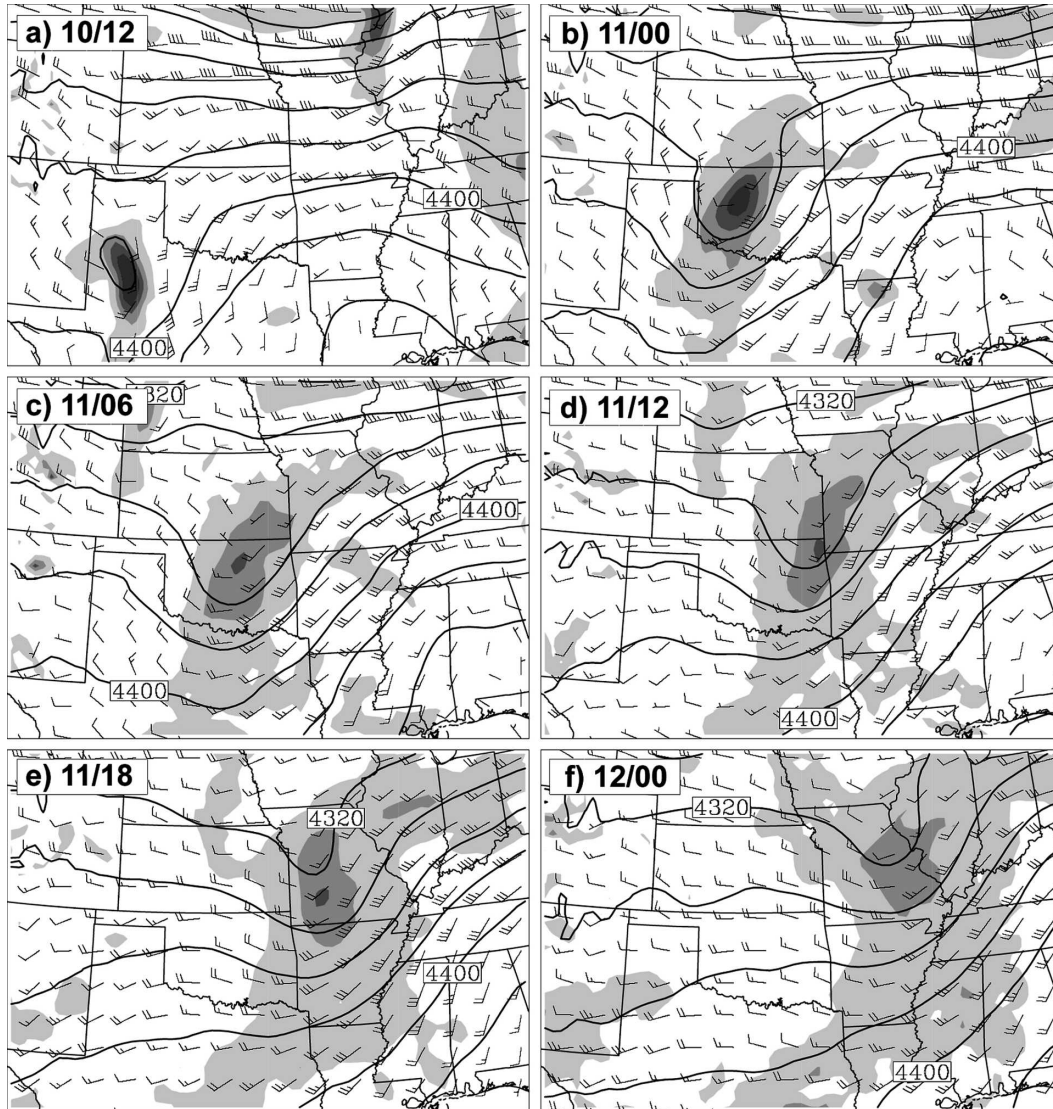


FIG. 6. Same as Fig. 3 but for the 10-km MM5 ensemble mean forecast.

4. Ensemble performance and error growth

a. Ensemble mean

The ensemble mean theoretically provides the most likely outcome of the future state of the atmosphere for an unbiased sample and with a perfect model, and the initial evolution of the event studied herein shows the ensemble mean to perform quite well. Figure 6 displays the ensemble mean forecast of 600-hPa wind, height, and PV at 1200 UTC 10 June and at 6-h intervals during the life cycle of the MCV of interest from 0000 UTC 11 June to 0000 UTC 12 June. Figures 6a–f correspond with the Eta 600-hPa analyses in Fig. 3. The forecast at 1200 UTC 10 June (Fig. 6a) shows a shortwave trough over the New Mexico/Texas border with an associated

mean PV maximum of over 2.0 PVU units (PVU, where $1 \text{ PVU} = 1.0 \times 10^{-6} \text{ m}^2 \text{ s}^{-1} \text{ K kg}^{-1}$) in west Texas. Despite slightly overpredicting the strength of the trough, this forecast verifies well with the 600-hPa Eta analysis in Fig. 3a. Figures 6b–d provide the ensemble mean forecasts of the 600-hPa flow pattern from 0000 to 1200 UTC 11 June and correspond to the time period beginning with MCS initiation (Fig. 2b) through the development of a well-defined MCV on radar (Fig. 2f). While the intensity of the 0000 UTC 11 June midlevel shortwave forecast by the ensemble mean in Fig. 6b verifies well with the 600-hPa analysis at that time (Fig. 3b), the ensemble mean performs poorly following the time of MCV formation (0600 UTC; Fig. 3c). For example, the ensemble mean does not depict the closed

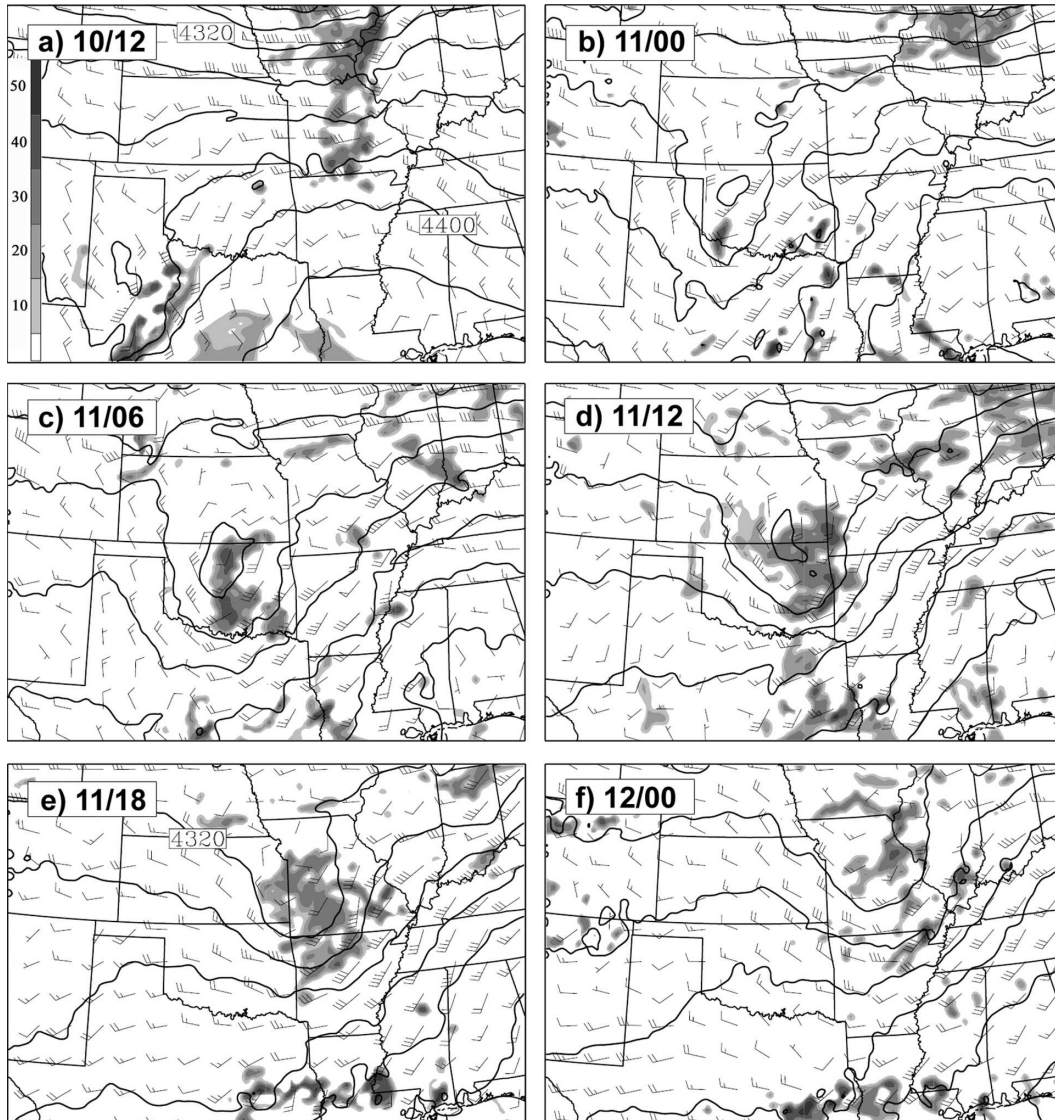


FIG. 7. The best ensemble member (EN-14) forecast of 600-hPa height (every 20 m), wind (full barb 5 m s^{-1}), and reflectivity (shaded every 10 dBZ) valid at (a) 1200 UTC 10 Jun 2003; (b) 0000, (c) 0600, (d) 1200, and (e) 1800 UTC 11 Jun 2003; and (f) 0000 UTC 12 Jun 2003.

circulation evident in the Eta analyses through 0000 UTC 12 June (Figs. 6c–f, 3c–f). In fact, the mean forecasts the wave to weaken through this time period whereas the analyses show a strengthening MCV. It is clear that until the time of MCV formation, the ensemble mean provides a good estimate of the midlevel flow pattern. After this time, ensemble spread becomes significant (described in the next section), and the best estimate no longer lies within the mean of the ensemble.

b. Error growth in the ensemble forecasts

Though the extent to which model error is responsible for the inaccuracy of the ensemble forecast is

unknown, the relatively accurate forecast from member EN-14 (see Fig. 7) suggests that the model is capable of producing a realistic MCV. For example, EN-14 correctly forecasts convection ahead of a midlevel trough over west Texas at 1200 UTC 10 June (Fig. 7a; compared to radar in Fig. 2b). Although EN-14 initiates convection roughly 6 h too late, it does forecast a developing MCS in Oklahoma at 0000 and 0600 UTC 11 June (Figs. 7b,c) that compares well to radar in Figs. 2d,f. Correspondingly, EN-14 forecasts a well-developed MCV, seen in the forecast of closed 600-hPa isoheights and a cyclonic circulation (Figs. 7c–f).

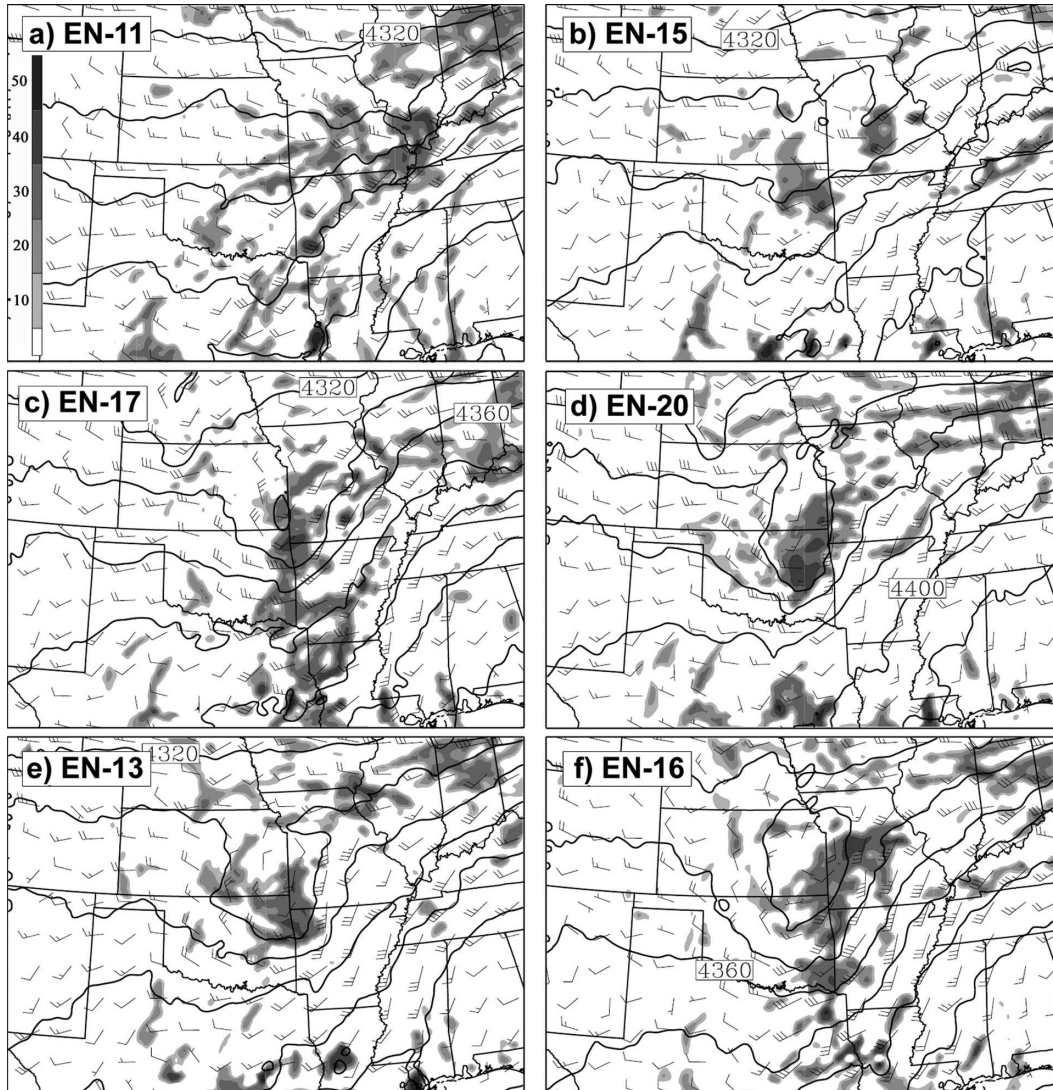


FIG. 8. The 600-hPa forecast of height (every 20 m), wind (full barb 5 m s^{-1}), and reflectivity (shaded every 10 dBZ) from six ensemble members: (a) EN-11, (b) EN-15, (c) EN-17, (d) EN-20, (e) EN-13, and (f) EN-16 valid at 1200 UTC 11 Jun 2003.

Although the initial conditions of the ensemble members differed only slightly, considerable spread developed within the ensemble in later forecasts. To exemplify the spread, the forecasts of six members are analyzed, among which EN-11 and EN-15 perform poorly, members EN-17 and EN-20 display fair performance, and EN-13 and EN-16 show forecasts nearest to observations. These 6 forecasts are given in Fig. 8, which provides 600-hPa height and wind along with reflectivity at 1200 UTC 11 June, when the MCV was well developed on radar over western Arkansas (Fig. 2f). EN-11 and especially EN-15 (Figs. 8a,b, respectively) do not forecast a significant midlevel disturbance at all and likewise do not forecast an organized convective

complex. On the other hand, members EN-17 and EN-20 (Figs. 8c,d, respectively) forecast an ongoing MCS at this time and an associated stronger 600-hPa trough. However, these two forecasts lack the closed circulation evident in the 600-hPa Eta analysis at that time (Fig. 3d), possibly because of delayed convective initiation. EN-13 and EN-16, on the other hand, forecast a mature MCS in Oklahoma 6 h earlier (not shown) and thus forecast a mature MCV with a closed circulation and weakening convection at 1200 UTC 11 June (Figs. 8e,f). It is noted that EN-13, which best resembles the observed MCV at 1200 UTC 11 June, also shows the best performance predicting the Oklahoma MCS at 0600 UTC 11 June. Those members who exhibit poor

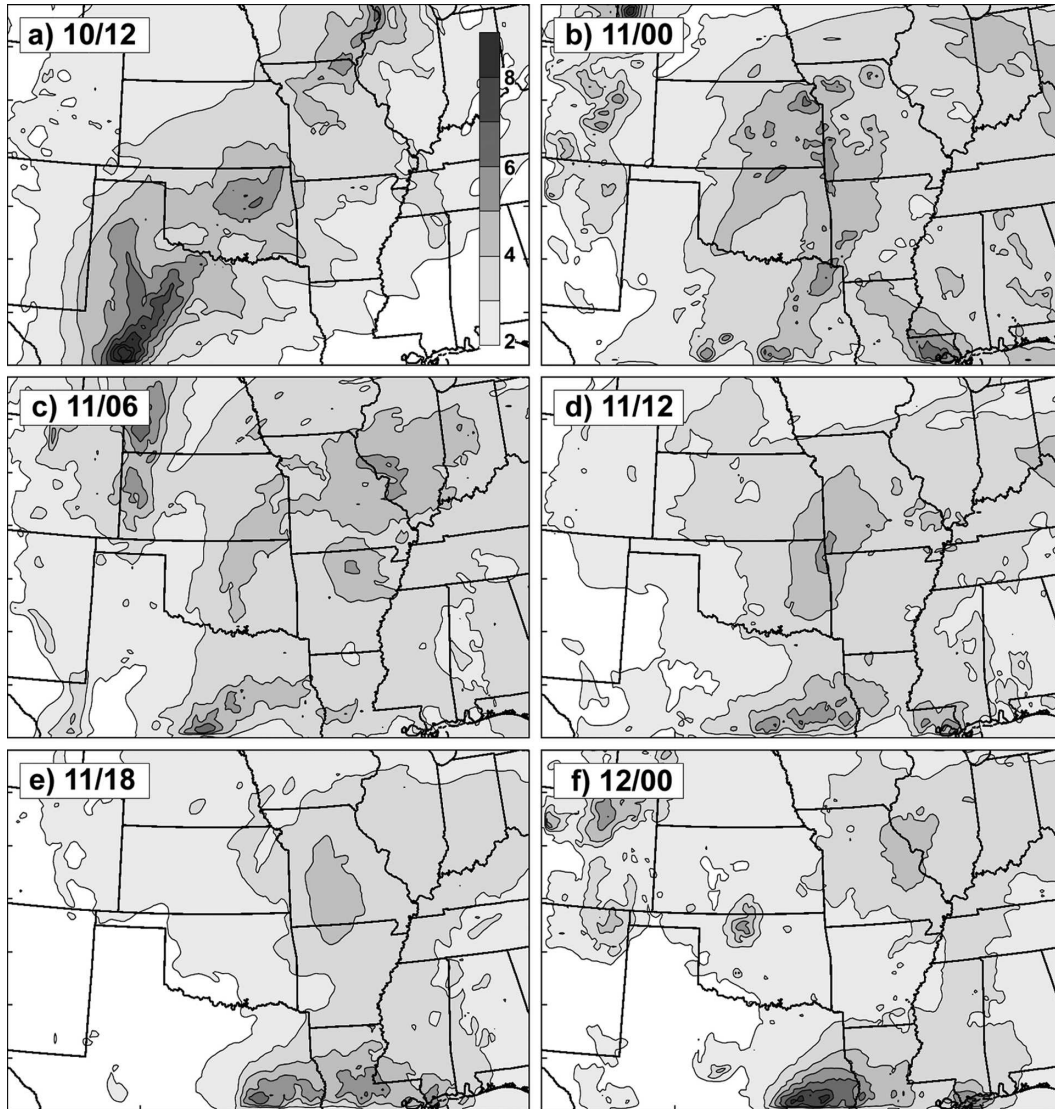


FIG. 9. Horizontal distribution of ensemble spread in terms of vertically averaged RM_DTE (every 1 m s^{-1}) valid at (a) 1200 UTC 10 Jun 2003; (b) 0000, (c) 0600, (d) 1200, and (e) 1800 UTC 11 Jun 2003; and (f) 0000 UTC 12 Jun 2003.

forecasts of the MCV at 1200 UTC 11 June also poorly forecast convection 6 h prior to that time, implying a dependence of the MCV predictability on the ability to predict the earlier MCS. Also, the relatively poor member forecasts were initialized with a weaker upper-level disturbance over the western United States at 0000 UTC 10 June (not shown).

The error growth and predictability of this MCV event can be quantified through examination of ensemble spread of the root-mean of difference total energy (RM_DTE), where

$$\text{DTE} = 0.5(u'u' + v'v' + kT'T'), \quad (1)$$

in which primes denote the difference between any member and the ensemble mean and $k = C_p/T_r$ ($C_p = 1004.9 \text{ J kg}^{-1} \text{ K}^{-1}$ and the reference temperature $T_r = 270 \text{ K}$; Zhang et al. 2003). Figure 9 gives the horizontal distribution of vertically averaged ensemble spread in terms of RM_DTE for 6-h intervals beginning at 1200 UTC 10 June, or 6 h after initialization, and at 6-h intervals following 0000 UTC 11 June corresponding with the times in Fig. 3. The initial RM_DTE due to the sample of the 3DVAR background error covariance is $\sim 1.0 \text{ m s}^{-1}$ throughout the model domain (not shown). The most significant regions of ensemble spread ($>5 \text{ m s}^{-1}$) through 0000 UTC 11 June (Figs. 9a,b) are

found in the immediate vicinity of moist convection and the midlevel shortwave trough. This relationship is consistent with the finding in Zhang et al. (2003) that moist convection is the key process in driving initial error growth. Beginning at 0600 UTC 11 June (Fig. 9c), roughly the time of MCV formation, a region of maximum ensemble spread greater than 4 m s^{-1} becomes associated with the MCV over central Oklahoma and reaches a maximum value of 5 m s^{-1} at 1200 UTC (Fig. 9d). After that time, RM_DTE slightly decreases following the MCV through the end of the forecast period. The local maxima in RM_DTE at the southernmost portion of the display domain and over the Front Range of the Rockies in Colorado (Figs. 9e,f) are related to diurnal convection in those areas and are not associated with the MCV.

The vertical distribution of horizontally averaged RM_DTE is analyzed in Fig. 10 in 6-h intervals (beginning with model initialization at 0000 UTC 10 June) and shows that convection likely had a significant impact on RM_DTE distribution. Initial error (between 1 and 1.5 m s^{-1}) is maximized in the upper and lower troposphere and is where RM_DTE grows most rapidly through 0000 UTC 11 June. At the same time, a third local error maximum grows in the midtroposphere between 0000 and 0600 UTC 11 June, centered between 500 and 600 hPa, the same layer where initial error was lowest. RM_DTE at this level peaks between 0000 and 0600 UTC 11 June, likely associated with the developing mean convection and the associated latent heating through that time (as well as a developing MCV in some members). The slight decrease in RM_DTE after 0600 UTC is attributed to the fact that many ensemble members do not forecast an MCV or widespread secondary convection after 1200 UTC 11 June; thus their forecasts are relatively similar (albeit bad).

The six chosen ensemble member forecasts presented in Fig. 8 and the DTE analyses in Figs. 9 and 10 illustrate the significant upscale error growth stemming from the slight variation in initial conditions. Subsequent error in larger-scale MCV forecasts appears to be directly related to uncertainty in the simulation of moist convection at all stages prior to the MCV formation. This result is comparable to error growth patterns seen within simulations of the 24–25 January 2000 snowstorm (Zhang 2005). Of particular interest is the forecast skill maintained by certain members throughout the development of the initial MCS and continuing through the penetration of the MCV circulation to the surface (not shown). As illustrated here, EN-13 and EN-16, which exhibit the best forecast of the initial MCS in Oklahoma, also accurately predict the MCV at 1200 UTC 11 June and the surface low at 0000 UTC 12

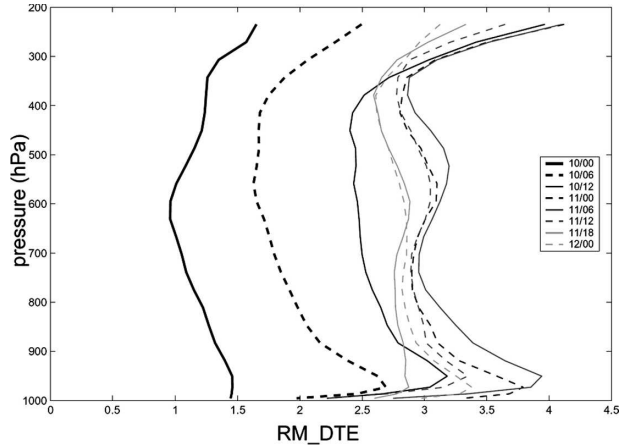


FIG. 10. Vertical distributions of horizontally averaged RM_DTE at 6-h intervals from 0000 to 1200 UTC 10 Jun 2003 and from 0000 UTC 11 Jun to 0000 UTC 12 Jun 2003.

June (not shown). At the same time, EN-11 and EN-15, which forecast very little convection at the time of the initial MCS, also exhibit very poor performances in forecasting the midlevel disturbance at 1200 UTC 11 June and at subsequent stages. These chosen ensemble member forecasts suggest the prominent role of moist convection in the predictability of this MCV and in the significant forecast divergence that results. However, the exact extent to which grid-scale convection is responsible for the forecast spread in this case is unknown. Other factors, such as the initialization of the upper-level disturbance, could certainly play a role as well.

5. Probabilistic evaluation of the MCV dynamics

Composite studies of observational data (e.g., Bartels and Maddox 1991; Trier et al. 2000b) provide important details about MCV dynamics but are limited by factors such as data availability and quantities unobserved or difficult to calculate (e.g., PV). For this reason, a composite set of numerical forecasts comes at a significant advantage. The flow-dependent error growth provides twenty different realizations with similar background conditions and allows for a detailed composite of MCV datasets. Dynamic trends and correlations can then be deduced from the composite data. On the other hand, the current ensemble method has its limitations since it is well known in statistics that correlation does not directly imply causality.

In this section, error correlation structure among the twenty ensemble members is evaluated to inspect the dynamics of the 10–13 June MCV. The correlation coefficient r is calculated among a set of N data points using

$$r(x_{i_1 j_1 k_1}, y_{i_2 j_2 k_2}) = \frac{\frac{1}{N-1} \sum_{n=1}^N (x_{i_1 j_1 k_1 n} - \overline{x_{i_1 j_1 k_1}})(y_{i_2 j_2 k_2 n} - \overline{y_{i_2 j_2 k_2}})}{\left[\frac{1}{N-1} \sum_{n=1}^N (x_{i_1 j_1 k_1 n} - \overline{x_{i_1 j_1 k_1}})^2 \right]^{1/2} \left[\frac{1}{N-1} \sum_{n=1}^N (y_{i_2 j_2 k_2 n} - \overline{y_{i_2 j_2 k_2}})^2 \right]^{1/2}}, \quad (2)$$

where x and y denote two model-state variables and i , j , and k are three-dimensional grid points. Correlations are examined among differing variables, spatial grid points (horizontal and vertical), and times, of which any may be held constant for the analysis. Also, to calculate correlation from a grid point in this study, a weighted average x_a is used in place of x and y in Eq. (2) with a weighting function f such that

$$x_a = \frac{1}{n} \sum_{i=1}^n (x_i f_i) \quad (3)$$

and

$$f_i = \frac{r_0^2 - r_i^2}{r_0^2}, \quad (4)$$

where x is a state variable, n is the number of averaged grid points, r_i is the distance from the center grid point, and r_0 is the maximum averaged radius, set at 210 km for all cases. In this study, a correlation of magnitude greater than 0.3 is considered weak, greater than 0.5 is moderate, and over 0.7 is high. The correlations examined in this section focus on the atmospheric processes that may be considered important to the 10–13 June MCV life cycle using a framework based on previous studies to be described in detail in subsequent subsections.

a. MCV precursor: West Texas MCS and resulting midlevel circulation

The influence of the early 10 June convection on the strength of the midlevel shortwave immediately preceding MCS initiation is examined in this section. It was discussed in section 2 that convection over west Texas and New Mexico during the early morning hours of 10 June may have amplified midlevel vorticity through the generation of mid- to upper-tropospheric latent heating and increased midlevel PV. This midlevel rotation is evident in radar loops through the time of convective initiation in Oklahoma (0000 UTC 11 June) and may have influenced the Oklahoma MCS and the subsequent MCV.

This part of the correlation study uses accumulated precipitation and surface temperature (lower temperatures are indicative of cold pools from more widespread convection) in order to represent convection during the

local morning of 10 June over New Mexico and Texas. While a more direct representation of convection through hydrometeors could also be used, the forecast surface cold pools generally encompass a larger area than localized convective updrafts and are detectable longer than hydrometeors. For this reason, surface temperatures are analyzed at 1200 UTC so that evaporative cooling effects of convection at any time up to that point may be included in the correlation analysis. The evaporative cooling within the ensemble members generally yields surface temperatures at or below 20°C at this time, in contrast to a temperature field averaging 25°C surrounding the respective cold pools. Therefore, radiational cooling at 1200 UTC is not considered to significantly detract from the surface temperature contrast needed for this analysis.

Figure 11 shows the 600-hPa PV at 0000 UTC 11 June and is meant to illustrate the mean structure of the midlevel shortwave around the time of convective initiation leading to the MCS (Fig. 2c). The ensemble mean PV is oriented in a southwest–northeast elongated manner from northwest Texas to eastern Kansas, along the center of the midlevel trough, and reaches a maximum of over 2.0 PVU over western Oklahoma. Additionally, the ensemble average surface temperature at 1200 UTC 10 June shows a negative anomaly of up to 6°C in west Texas where convection is most common among ensemble members at 0900 and 1200 UTC.

The relationship between the west Texas convection and the subsequent midlevel shortwave at 0000 UTC 11 June is investigated in Fig. 11. The correlation between 0000 UTC 11 June 600-hPa PV at point A and the surface temperature field 12 h earlier is shown in Fig. 11a. A moderate-to-high negative correlation (< -0.6) exists over a large part of western Texas and eastern New Mexico. This correlation pattern is indicative of a connection between convection at 1200 UTC and the strength of the midlevel vortex 12 h later. In addition, the expanse of the negative correlation to the north and west indicates that a stronger midlevel vortex is also related to convection that initiates earlier and farther northwest. Figure 11b shows a similar correlation analysis to Fig. 11a, but 12-h accumulated precipitation at 1200 UTC is used instead of surface temperature. The correlation pattern in Fig. 11b, with a moderate positive correlation (> 0.6) over west Texas that ex-

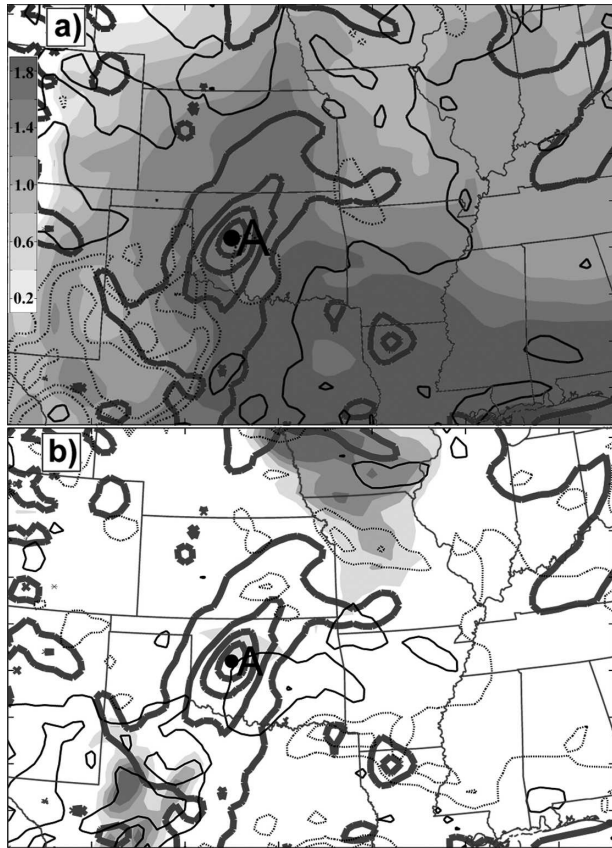


FIG. 11. (a) Correlations between the 600-hPa PV at point A at 0000 UTC 11 Jun 2003 and surface temperature at 1200 UTC 10 Jun 2003 (black contours; every 0.2 from ± 0.3 ; negative, dashed). Also displayed are the 600-hPa ensemble mean PV (thick gray contours; every 0.5 PVU) at 0000 UTC 11 Jun 2003 and surface temperature (shaded every 2°C) at 1200 UTC 10 Jun 2003. (b) Correlations between the 600-hPa PV at point A at 0000 UTC 11 Jun 2003 and 12-h accumulated precipitation at 1200 UTC 10 Jun 2003 [contours as in (a); mean shaded every 4 mm].

tends westward into New Mexico, is similar to that shown in Fig. 11a and verifies the correlation using surface temperature. Additionally, various reverse correlations between the 1200 UTC surface temperature field and the PV field at 0000 UTC 11 June indicate that stronger and more widespread convection during the morning of 10 June correlates with a stronger and narrower vortex focused in the midlevels (not shown).

The correlations in Fig. 11 are exemplified in Fig. 12 by comparing the 1200 UTC 10 June reflectivity, 12-h accumulated precipitation, and surface temperature forecasts of EN-11 and EN-13 (Figs. 12a,b, respectively) to their respective 600-hPa PV forecasts 12 h later (Figs. 12c,d). EN-11 forecasts weaker convection over a more constrained area than does EN-13 (as seen by their accumulated precipitation forecasts), and consequently its forecast surface cold pool is much smaller.

Similar to its limited forecast of convection, EN-11 forecasts a much weaker and broader PV anomaly at 0000 UTC, with the PV maximum actually focused ahead of the midlevel trough in the vicinity of weak convection (not shown). Conversely, EN-13 forecasts more widespread convection at 1200 UTC, and its forecast PV at 0000 UTC is significantly stronger and more concentrated along the base of the midlevel shortwave. Similar to EN-13, EN-14 forecasts widespread convection at 1200 UTC 10 June over western Texas (Fig. 7a) and a stronger midlevel disturbance over Oklahoma at 0000 UTC 11 June (Fig. 7b).

To determine the direction of the cause and effect relationship, Fig. 13 gives the correlation between the 0000 UTC 11 June 600-hPa PV at point A and the 250-hPa PV at 0900 UTC 10 June, the time at which most ensemble members (about 13) initiate convection ahead of the initial upper-level disturbance. A strong positive correlation of almost 0.7 exists over the upper-level wave, and a negative correlation is to its east. A vertical cross section (Fig. 13b) shows that the midlevel wave at 0000 UTC 11 June is positively correlated with a weak midtropospheric PV anomaly that exists immediately ahead of the upper-level wave at 0900 UTC 10 June. This relative PV maximum exists where most ensemble members initiate convection at or before 0900 UTC 10 June and is positively correlated with the 0000 UTC midlevel vortex. An area of negative correlation is located directly above the lead PV anomaly in the upper troposphere, where a convectively driven negative PV perturbation would be expected. Additional correlation analyses (not shown) suggest that a stronger upper wave at 0900 UTC 10 June is positively correlated with stronger and more widespread convection during the morning hours of 10 June that then correlates with a stronger midlevel vortex that evening, consistent with Galarneau and Bosart (2004). The correlations in Figs. 10 and 12 suggest that a stronger midlevel shortwave at 0000 UTC 11 June is correlated with a stronger upper-level disturbance at 0900 UTC 10 June via the enhancement of convection during the morning hours of 10 June and may not be simply the translation of stronger PV through time.

b. 0000 UTC 11 June shortwave and 1200 UTC 11 June MCV

Past studies have demonstrated that the presence of midlevel vorticity with magnitude exceeding the local Coriolis parameter may be beneficial to the organization of convection leading to an MCV. For example, a numerical study by Davis and Weisman (1994) found that in the presence of ambient vorticity, mesoscale or larger-scale balanced vortices were favored as opposed

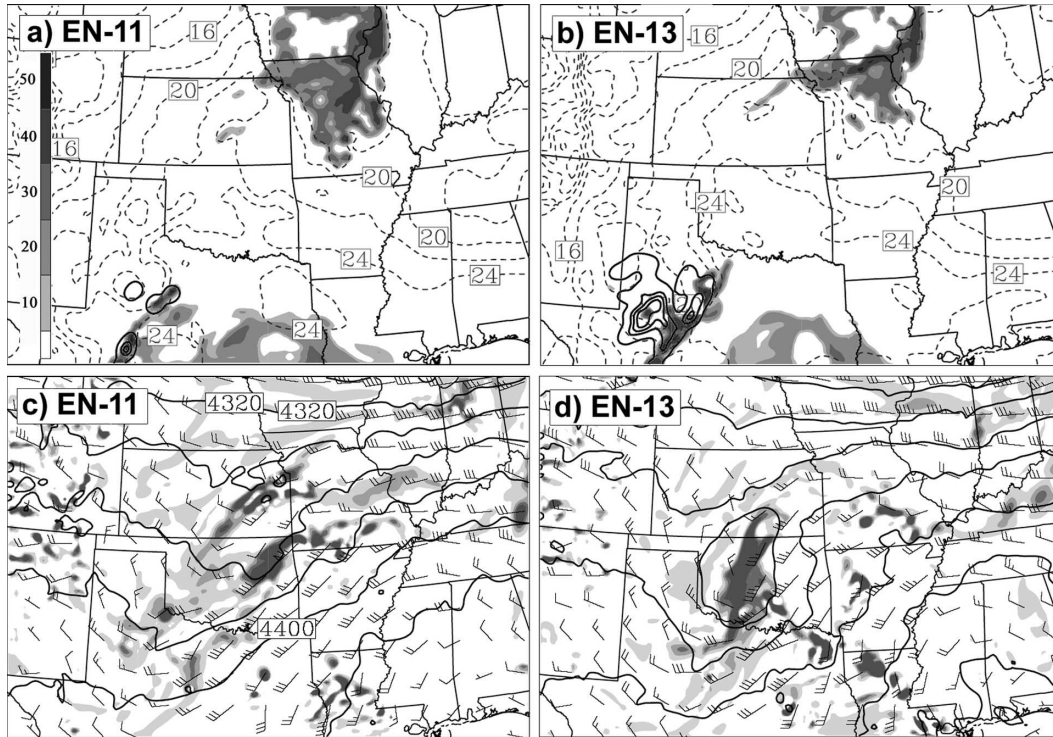


FIG. 12. Ensemble member (a) EN-11 and (b) EN-13 forecasts of reflectivity (shaded every 10 dBZ), surface temperature (dashed contours every 4°C), and 12-h accumulated precipitation over the area of interest (black contours every 10 mm) at 1200 UTC 10 Jun 2003. The 600-hPa PV (shaded every 0.5 PVU), height (every 10 m), and wind (full barb 5 m s^{-1}) from (c) EN-11 and (d) EN-13 at 0000 UTC 11 Jun 2003.

to smaller bookend vortices. Additionally, numerous tropical cyclone studies (e.g., Riehl 1948, 1950; Gray 1968; Harr et al. 1996a,b; Zhang and Bao 1996a,b) noted the importance of a preexisting disturbance that may act to organize convection and eventually lead to an organized disturbance. Using a PV approach in a modeling study of Hurricane Diana (in 1984), Davis and Bosart (2001) found that low-level, convectively induced PV anomalies were able to merge into a large, coherent maximum in the presence of a parent vorticity center. These studies demonstrated the significance of ambient vorticity to MCV development, which is the subject of the correlation analysis in this subsection.

The correlation pattern in Fig. 14, which is meant to determine the connection between a preexisting vortex and MCV formation in the case of 11 June, supports the concept of preexisting vorticity as an important factor to MCV development. Figure 14a shows the correlation between the 600-hPa vorticity at 0000 UTC 11 June at point A and the 600-hPa PV field 12 h later. It is around the latter time that most ensemble members forecast a mature MCV (11 of the 14 members that forecast a closed circulation). A positive correlation of over 0.5 is shown near and slightly west of the maximum PV, sug-

gesting that a stronger midlevel vortex yields a stronger midlevel PV disturbance at 1200 UTC.

Similarly, the correlation between 600-hPa PV at 1200 UTC 11 June at point B (denoted in Fig. 14) and the 600-hPa vorticity field 12 h earlier suggests that the stronger MCV is correlated with a stronger initial midlevel shortwave as a moderate, positive correlation is associated with the center of the strongest 0000 UTC 11 June midlevel vortex. This correlation pattern is supported by the individual ensemble forecasts of 600-hPa relative vorticity at 0000 UTC 11 June (Figs. 15a,b) and 600-hPa PV at 1200 UTC 11 June (Figs. 15c,d). Member EN-13 forecasts a coherent and well-organized vorticity maximum accompanying a relatively large midlevel shortwave trough at 0000 UTC 11 June (Fig. 15b), whereas EN-11 places the vorticity maximum to the east of the shortwave trough axis in the vicinity of weak convection and does not suggest the balanced pattern evident in EN-13 (Fig. 15a). Accordingly, member EN-13 forecasts a spatially coherent PV perturbation 12 h later (Fig. 15d), whereas EN-11 forecasts small-scale anomalies in the vicinity of weak convection (not shown) and lacks a widespread or well-defined vortex (Fig. 15c). In a similar manner, the relatively strong

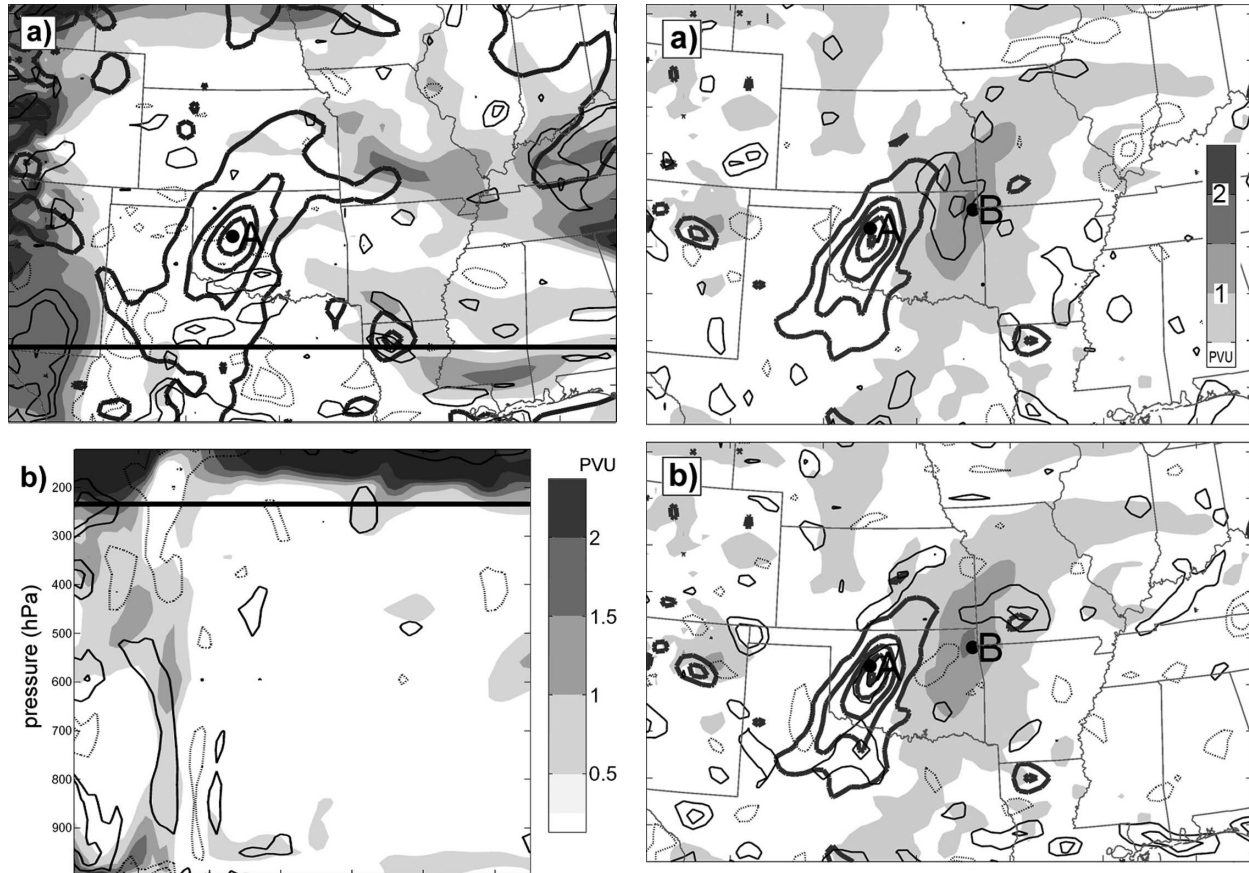


FIG. 13. (a) Correlations between the 600-hPa PV at point A at 0000 UTC 11 Jun and the 250-hPa PV at 0900 UTC 10 Jun (black contours; every 0.2 from ± 0.3 ; negative, dashed). Also displayed are the 600-hPa ensemble mean PV at 0000 UTC 11 Jun (contoured in thick gray every 0.5 PVU) and the 250-hPa ensemble mean PV at 0900 UTC 10 Jun (shaded). (b) Correlations between the 600-hPa PV at point A at 0000 UTC 11 Jun and the PV at 0900 UTC 10 Jun [contours as in (a)] along the cross section [black line in (a)]. Also displayed is the ensemble mean PV at 0900 UTC 10 Jun (shaded).

midlevel shortwave trough forecast by EN-14 at 0000 UTC 11 June (Fig. 7b) deepens into a closed midlevel circulation at 1200 UTC (Fig. 7d) via strong, organized convection (Figs. 7c,d). Though the precise processes that are responsible for this relationship cannot be determined, it is likely that a stronger trough and its associated quasi-balanced vertical motions would increase the magnitude of convective heating and affect the correlation pattern in Fig. 14.

c. Secondary convection, midlevel vortex strength, and surface vortex growth

Several processes can act simultaneously in order to deepen a midtropospheric vortex so that it may reach

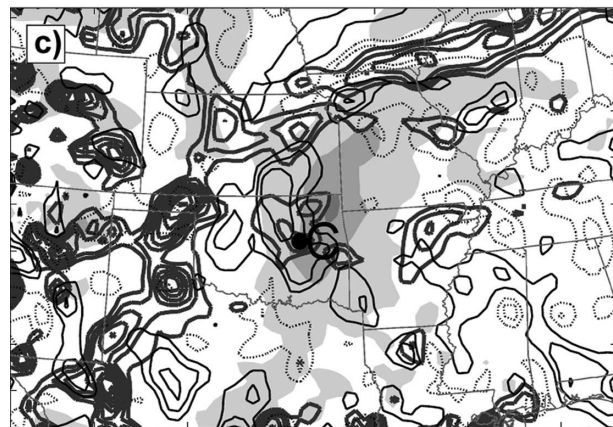


FIG. 14. Correlations (black contours; every 0.2 from ± 0.3 ; negative, dashed) between (a) the 600-hPa relative vorticity at point A at 0000 UTC 11 Jun 2003 and the 600-hPa PV at 1200 UTC 11 Jun 2003, (b) the 600-hPa PV at point B at 1200 UTC 11 Jun 2003 and the 600-hPa relative vorticity at 1200 UTC 11 Jun 2003, and (c) the surface vorticity at point C at 1200 UTC 11 Jun 2003 and the 600-hPa PV at 1200 UTC 11 Jun 2003. Also displayed are the corresponding ensemble mean relative vorticity (thick gray contours; every $5 \times 10^{-5} \text{ s}^{-1}$) and 600-hPa PV shaded every 0.5 PVU.

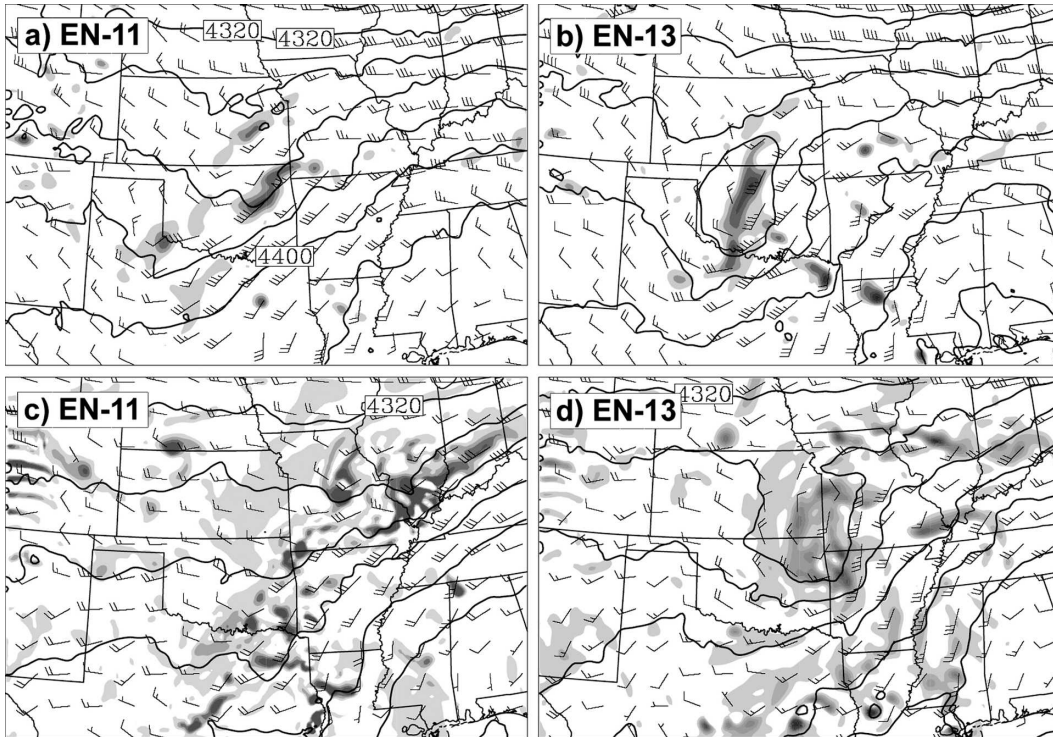


FIG. 15. Ensemble member (a) EN-11 and (b) EN-13 forecasts of height (every 20 m), wind (full barb 5 m s^{-1}), and 600-hPa relative vorticity (shaded every $5 \times 10^{-5} \text{ s}^{-1}$) valid at 0000 UTC 11 Jun 2003. The 600-hPa PV (shaded every 0.5 PVU), height (every 10 m), and wind (full barb 5 m s^{-1}) from (c) EN-11 and (d) EN-13 at 1200 UTC 11 Jun 2003.

the surface. For example, Ritchie and Holland (1997) found that a PV merger process similar to that described by Davis and Bosart (2001), as well as increasing background vorticity, can act to increase the Rossby–Burger–Prandtl penetration depth (Hoskins et al. 1985) and lead to a deeper vortex that may penetrate to the surface. In an observational study, Fritsch et al. (1994) speculated that the penetration depth would be further increased by the amplification of the midlevel PV anomaly through the development of subsequent convection within the vortex. This concept was supported by a modeling study of Rogers and Fritsch (2001), who found that an MCV strengthened and spread to the lower troposphere in response to mid- and upper-tropospheric warming created by such convection. They noted that the heating took place within a saturated layer resulting from mesoscale ascent as a low-level jet of high- θ_e air was forced to rise over a low-level cold pool, as is characteristic of many MCVs. This moist, near-neutral layer sufficiently reduced the Rossby radius of influence such that latent heating was retained and the vortex was able to penetrate into the surface cold pool, resulting in lowered heights and a cyclonic circulation at the surface. Additionally, Trier

et al. (2000a) found in a numerical study that low-level vertical ascent is favored on the downshear flank of an MCV with descent upshear, consistent with the conceptual MCV model of Raymond and Jiang (1990, their Fig. 2). It was observed in Trier et al. (2000a) that the maximum upward displacements occurred near the radius of maximum winds and ranged from downshear for moderately strong vortices in strong shear to 90° to the left of downshear for strong vortices in weak shear. Shear-induced tilting then placed the location of maximum vertical displacements close to the center of the vortex at the level of maximum vortex strength. This could provide an environment more favorable for convection near the MCV center. They also found that strong vortices of moderate-to-large size are more likely to be associated with deeper low-level ascent and could likewise be more favorable for secondary convection.

The speculated importance of convection to the development of a surface vortex motivates an examination of the relationship between the strength of the 11 June MCV, its subsequent convection, and the surface vortex development. A Lagrangian coordinate system centered on the midlevel circulation center for each

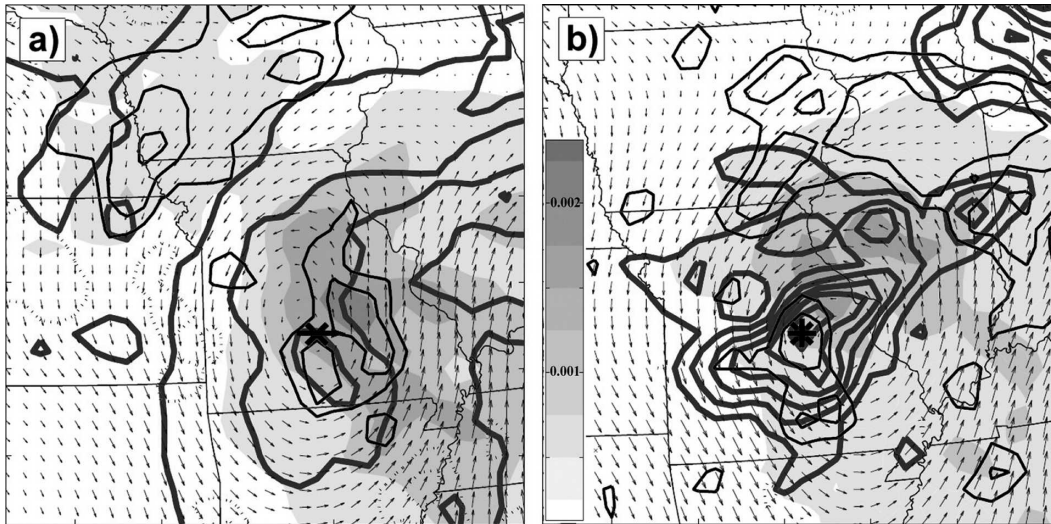


FIG. 16. (a) Correlations (black contours; every 0.2 from ± 0.3 ; negative, dashed) between the 600-hPa PV at the MCV center (denoted by an x) and the column-integrated QPR at 1800 UTC 11 Jun 2003 with the corresponding ensemble mean PV contoured in thick gray every 0.5 PVU and ensemble mean QPR shaded every $0.5 \times 10^{-3} \text{ g kg}^{-1}$. (b) Correlations between the surface relative vorticity at the MCV center (denoted by an x) and the column-integrated QPR at 0000 UTC 12 Jun 2003 with the corresponding ensemble mean surface vorticity contoured in thick gray every $2.5 \times 10^{-5} \text{ s}^{-1}$ and ensemble mean QPR shaded every $0.5 \times 10^{-3} \text{ g kg}^{-1}$. The ensemble mean and correlations are estimated in a Lagrangian framework relative to the MCV center. Map is overlain to depict scale and approximate mean MCV location. The ensemble mean 2.0–6.0-km shear vector is depicted by a boldface arrow over the MCV center in (a), and MCV-relative 600-hPa winds at both times are depicted with arrows.

member is used for correlation analysis during this stage of the MCV. This coordinate system is used since variability among ensemble members is much greater at this stage, and the vortex position varies by over 100 km. Such large position differences cannot be compensated for by the simple weighted average used in the previous analyses. Additionally, the six members that failed to produce significant convection or an MCV circulation overnight on 11 June are omitted from the analysis at this time, because their forecasts are the least useful to the investigation of MCV dynamics involving subsequent convection. Using the Lagrangian method, 600-hPa PV is examined to represent the strength of the MCV at the time at which the ensemble mean PV is strongest (1800 UTC 11 June). To find the Lagrangian vortex center, 600-hPa MCV-relative winds are computed by subtracting the mean phase speed of the MCV (8 m s^{-1} , 240°) at this time. Finally, shear-relative quadrants are determined by calculating the 2–6-km shear vector ($1.57 \times 10^{-3} \text{ s}^{-1}$, 270°), which is averaged over a 210-km radius and centered on each MCV.

The results shown in Fig. 16a support several findings of Trier et al. (2000a). This figure displays the correlation between PV at the MCV-relative circulation center and precipitation, represented by column-integrated hydrometeor mixing ratio (QPR). The maximum mean

precipitation is displaced roughly 50–100 km northeast of the MCV center on the left downshear flank of the vortex. This precipitation pattern corresponds with developing convection slightly north of the actual MCV center in Fig. 2h and is consistent with the finding of Trier et al. (2000a) that maximum vertical displacements are favored up to 90° to the left of downshear. At this time, widespread positive correlation between the PV at the circulation center and QPR is seen over the downshear flank of the circulation with moderate positive correlation located close to the maximum mean QPR and over the maximum mean PV. Areas of significant positive correlation are also shown along the western and northern peripheries of the area of mean convection. This correlation further supports the findings of Trier et al. (2000a) that stronger vortices are more favorable to secondary convection.

Several complicating factors likely influence the precipitation patterns in Fig. 16. First, the positive correlation to the right of downshear may be attributable to the fact that little to no convective inhibition is forecast by the ensemble members at this time (not shown). In addition, all members forecast a nearly saturated lower troposphere along the southern and eastern quadrants of the MCV. With little lifting needed to initiate convection, parcels in this quadrant likely do not need to travel to the left downshear quadrant for convection to

initiate. In addition, the high instability and low vertical shear of the MCV environment, as well as the existence of several outflow boundaries, play a complicating role in the type, intensity, and location of convection (not shown). Convective initiation due to these factors is indistinguishable from that due to the shear/vortex interaction mechanism in this analysis.

The relationship between convection and surface vortex growth is evaluated by calculating the correlation coefficient between the surface vorticity at 0000 UTC 12 June (the time at which the ensemble mean surface vortex is strongest) and convection. Figure 16b presents the correlation between the surface vorticity at 0000 UTC 12 June at the point of maximum mean (denoted by an “x”) and the precipitation field at the same time, represented by QPR. A moderately strong positive correlation of over 0.5 exists over the mean surface vortex and is consistent with studies that suggest convection in this location is most favorable for surface vortex development (e.g., Fritsch et al. 1994; Rogers and Fritsch 2001). This positive correlation is enhanced by the fact that all members that produce a surface vortex forecast nearly saturated low levels near the MCV center (not shown). In such a case, convective downdrafts may not be as efficient in cooling the lower troposphere, which would act to counter the surface pressure falls. Low-level saturation also favors PV generation and a surface vortex in the lower troposphere. The relationship between convection and a surface vortex is also supported in Fig. 14c, which provides an analysis of surface vorticity at 1200 UTC 11 June during the MCV formation stage. Though only four members forecast a surface vortex at this time, a strong positive correlation exists between the surface vorticity at point C and midlevel PV to the west of the surface vortex. This surface vorticity develops in response to widespread convection forecast downshear of a midlevel PV anomaly near the region of high correlation (convection not shown).

The results in Fig. 17 further support the notion that a surface vortex is favored in the vicinity of convection near the MCV center. This figure shows a closer look at the correlation in Fig. 16b with a scatterplot of averaged ensemble surface vorticity versus averaged QPR at point x (in Fig. 16b). A significant correlation coefficient of 0.77 is measured at that point, illustrating a defined relationship between the strength of the horizontally averaged surface vortex to averaged convection directly overhead among ensemble members. A diagnosis of low-level PV generation would be needed to investigate the cause of this relationship but is beyond the scope of this study.

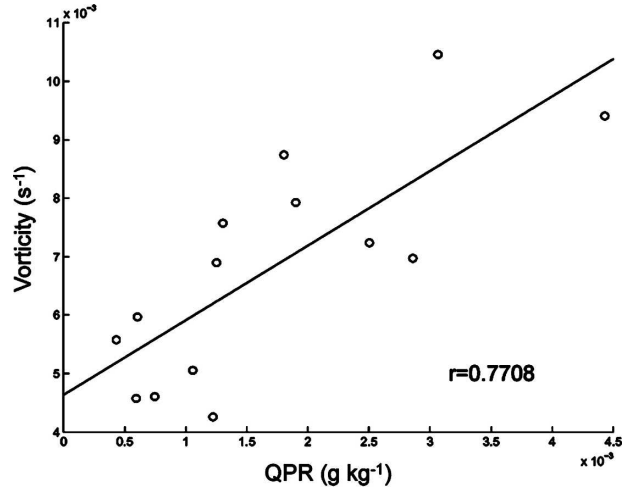


FIG. 17. Scatterplot and correlation between surface relative vorticity (s^{-1}) and QPR ($g\ kg^{-1}$) at the MCV center (point x in Fig. 16b) at 0000 UTC 12 Jun 2003.

6. Summary and discussion

This study introduces ensemble forecasting into the ongoing exploration of MCV dynamics through a case study of the long-lived MCV of 10–13 June 2003. The extreme sensitivity of such an MCV to numerous convective cycles is demonstrated, as slight perturbations in initial conditions escalate into significant forecast errors throughout the MCV life cycle in the presence of moist convection. Convection from as early as the local morning of 10 June is shown to have a significant impact on all stages of the MCV life cycle. Through diabatically induced PV perturbations, stronger convection in west Texas is shown to strengthen the existing midlevel shortwave, and a stronger wave in turn yields stronger and more widespread convection in Oklahoma, which then results in a stronger MCV. It is also shown that a stronger MCV favors secondary convection, which in turn allows vortex penetration to the surface. The extreme sensitivity of each of these processes to preceding moist convection events results in a large ensemble spread and a great deal of forecast uncertainty regarding the life cycle of an MCV.

The discrepancy among ensemble members allows for an investigation of MCV dynamics through the analysis of various ensemble forecasts, both in case-by-case (member-by-member) and statistical manners. Ensemble forecasts verify that an existing disturbance prior to MCS initiation correlates with a stronger MCV, a result that is consistent with the findings of past tropical and midlatitude studies. It is also shown that during the local daytime hours following MCV formation, forecasted precipitation is most commonly concen-

trated along the downshear periphery of the MCV. Furthermore, the ensemble correlation analyses suggest that a stronger MCV during this stage is more conducive to secondary convection, particularly close to and downshear of the MCV center near the radius of maximum winds. These findings support the hypothesis of Trier et al. (2000a). A significant positive relationship between the strength of secondary convection and surface vorticity during the subsequent diurnal cycle is found, though it is hard to determine the underlying cause of this correlation. Nonetheless, the findings support previous studies that hypothesize midtropospheric convective warming to be a potential source for surface vortex growth.

This study provides a general overview of MCV dynamics by exploiting the disparity among ensemble forecasts. A similar set of forecasts can come at a significant advantage for a more detailed dynamic investigation, such as the vorticity budget analysis of two MCVs performed by Kirk (2003). It is emphasized that the results presented in this study are derived from only one particular MCV event. The varied nature of ways an MCV may form and evolve in various synoptic environments illustrates the importance of examining a wide range of MCVs. The use of ensemble forecasting in this study proves to be of significant value in understanding the dynamics and predictability of this MCV event. Applying these methods to subsequent MCV cases will broaden the awareness of MCV dynamics and lead to a better understanding of the extent to which these systems can accurately be predicted.

Acknowledgments. This research was completed as part of D. P. Hawblitzel's master's thesis at the Texas A&M University. It is supported by NSF Grant ATM-0205599 and by the Office of Navy Research under the Young Investigator Program (Award 000140410471). The authors acknowledge John Nielsen-Gammon, Craig Epifanio, Robert Hetland, Lance Bosart, Jason Sippel, and Tom Galarneau for comments beneficial to this study.

REFERENCES

- Barker, D. M., W. Huang, Y. R. Guo, A. J. Bourgeois, and Q. N. Xiao, 2004: A three-dimensional variational data assimilation system for MM5: Implementation and initial results. *Mon. Wea. Rev.*, **132**, 897–914.
- Bartels, D. L., and R. A. Maddox, 1991: Mid-level cyclonic vortices generated by mesoscale convective systems. *Mon. Wea. Rev.*, **119**, 104–118.
- Bosart, L. F., and F. Sanders, 1981: The Johnstown flood of July 1977: A long-lived convective system. *J. Atmos. Sci.*, **38**, 1616–1642.
- Buizza, R., and P. Chessa, 2002: Prediction of the U.S. storm of 24–26 January 2000 with the ECMWF ensemble prediction system. *Mon. Wea. Rev.*, **130**, 1531–1551.
- Cohn, S. E., 1997: An introduction to estimation theory. *J. Meteor. Soc. Japan*, **75**, 257–288.
- , and D. F. Parrish, 1991: The behavior of forecast error covariances for a Kalman filter in two dimensions. *Mon. Wea. Rev.*, **119**, 1757–1785.
- Cotton, W. R., M.-S. Lin, R. L. McAnelly, and C. J. Tremback, 1989: A composite model of mesoscale convective complexes. *Mon. Wea. Rev.*, **117**, 765–783.
- Daley, R., 1992: Estimating model-error covariances for applications to atmospheric data assimilation. *Mon. Wea. Rev.*, **120**, 1735–1746.
- Davis, C. A., and M. L. Weisman, 1994: Balanced dynamics of mesoscale vortices produced in simulated convective systems. *J. Atmos. Sci.*, **51**, 2005–2030.
- , and L. F. Bosart, 2001: Numerical simulations of the genesis of Hurricane Diana (1984). Part I: Control simulation. *Mon. Wea. Rev.*, **129**, 1859–1881.
- , and S. B. Trier, 2002: Cloud-resolving simulations of mesoscale vortex intensification and its effect on a serial mesoscale convective system. *Mon. Wea. Rev.*, **130**, 2839–2858.
- , and S. B. Trier, 2007: Mesoscale convective vortices observed during BAMEX. Part I: Kinematic and thermodynamic structure. *Mon. Wea. Rev.*, in press.
- , D. A. Ahijevych, and S. B. Trier, 2002: Detection and prediction of warm season midtropospheric vortices by the Rapid Update Cycle. *Mon. Wea. Rev.*, **130**, 24–42.
- , and Coauthors, 2004: The Bow Echo and MCV Experiment: Observations and opportunities. *Bull. Amer. Meteor. Soc.*, **85**, 1075–1093.
- Dudhia, J., 1993: A nonhydrostatic version of the Penn State–NCAR Mesoscale Model: Validation tests and simulation of an Atlantic cyclone and cold front. *Mon. Wea. Rev.*, **121**, 1493–1513.
- Evensen, G., 1994: Sequential data assimilation with a nonlinear quasi-geostrophic model using Monte Carlo methods to forecast error statistics. *J. Geophys. Res.*, **99** (C5), 10 143–10 162.
- Fritsch, J. M., J. D. Murphy, and J. S. Kain, 1994: Warm core vortex amplification over land. *J. Atmos. Sci.*, **51**, 1780–1807.
- Galarneau, T. J., Jr., and L. F. Bosart, 2004: The long-lived MCV of 11–13 June 2003 during BAMEX. Preprints, *22d Conf. on Severe Local Storms*, Hyannis, MA, Amer. Meteor. Soc., CD-ROM, 5.4.
- Gray, W. M., 1968: Global view of the origin of tropical disturbances and storms. *Mon. Wea. Rev.*, **96**, 669–700.
- Grell, G. A., 1993: Prognostic evaluation of assumptions used by cumulus parameterizations. *Mon. Wea. Rev.*, **121**, 5–31.
- Harr, P. A., R. L. Elsberry, and J. C. L. Chan, 1996a: Transformation of a large monsoon depression to a tropical storm during TCM-93. *Mon. Wea. Rev.*, **124**, 2625–2643.
- , M. S. Kalafsky, and R. L. Elsberry, 1996b: Environmental conditions prior to formation of a midlevel tropical cyclone during TCM-93. *Mon. Wea. Rev.*, **124**, 1693–1710.
- Haynes, P. H., and M. E. McIntyre, 1987: On the evolution of vorticity and potential vorticity in the presence of diabatic heating and frictional or other forces. *J. Atmos. Sci.*, **44**, 828–841.
- Hoskins, B. J., M. E. McIntyre, and A. W. Robertson, 1985: On the use and significance of isentropic potential vorticity maps. *Quart. J. Roy. Meteor. Soc.*, **111**, 877–946.
- Jiang, H., and D. J. Raymond, 1995: Simulation of a mature me-

- mesoscale convective system using a nonlinear balance model. *J. Atmos. Sci.*, **52**, 161–175.
- Kirk, J. R., 2003: Comparing the dynamical development of two mesoscale convective vortices. *Mon. Wea. Rev.*, **131**, 862–890.
- Lorenz, E. N., 1969: The predictability of a flow which possesses many scales of motion. *Tellus*, **21**, 289–307.
- Mellor, G. L., and T. Yamada, 1982: Development of a turbulence closure model for geophysical fluid problems. *Rev. Geophys. Space Phys.*, **20**, 851–875.
- Menard, R. D., and J. M. Fritsch, 1989: An MCC-generated inertially stable warm core vortex. *Mon. Wea. Rev.*, **117**, 1237–1261.
- Molteni, F., R. Buizza, T. N. Palmer, and T. Petroliaigis, 1996: The ECMWF ensemble prediction system. Methodology and validation. *Quart. J. Roy. Meteor. Soc.*, **122**, 73–119.
- Montgomery, M. T., and J. Enagonio, 1998: Tropical cyclogenesis via convectively forced vortex Rossby waves in a three-dimensional quasigeostrophic model. *J. Atmos. Sci.*, **55**, 3176–3207.
- Nielsen-Gammon, J. W., F. Zhang, A. M. Odins, and B. Myoung, 2005: Extreme rainfall in Texas: Patterns and predictability. *Phys. Geogr.*, **26**, 340–364.
- Raymond, D. J., and H. Jiang, 1990: A theory for long-lived mesoscale convective systems. *J. Atmos. Sci.*, **47**, 3067–3077.
- Reisner, J., R. J. Rasmussen, and R. T. Bruintjes, 1998: Explicit forecasting of supercooled liquid water in winter storms using the MM5 Mesoscale Model. *Quart. J. Roy. Meteor. Soc.*, **124B**, 1071–1107.
- Riehl, R. J., 1948: On the formation of typhoons. *J. Meteor.*, **5**, 247–264.
- , 1950: A model of hurricane formation. *J. Appl. Phys.*, **21**, 917–925.
- Ritchie, E. A., and G. J. Holland, 1997: Scale interactions during the formation of typhoon Irving. *Mon. Wea. Rev.*, **125**, 1377–1396.
- Rogers, R. F., and J. M. Fritsch, 2001: Surface cyclogenesis from convectively driven amplification of midlevel mesoscale convective vortices. *Mon. Wea. Rev.*, **129**, 605–637.
- Snyder, C., and F. Zhang, 2003: Assimilation of simulated Doppler radar observations with an ensemble Kalman filter. *Mon. Wea. Rev.*, **131**, 1663–1677.
- Talagrand, O., 1997: Assimilation of observations, an introduction. *J. Meteor. Soc. Japan*, **75**, 191–209.
- Thorpe, A. J., 1985: Diagnosis of balanced vortex structure using potential vorticity. *J. Atmos. Sci.*, **42**, 397–406.
- Toth, Z., and E. Kalnay, 1997: Ensemble forecasting at NCEP and the breeding method. *Mon. Wea. Rev.*, **125**, 3297–3319.
- Tracton, M. S., and E. Kalnay, 1993: Operational ensemble prediction at the National Meteorological Center: Practical aspects. *Wea. Forecasting*, **8**, 379–400.
- Trier, S. B., and C. A. Davis, 2002: Influence of balanced motions on heavy precipitation within a long-lived convectively generated vortex. *Mon. Wea. Rev.*, **130**, 877–899.
- , —, and W. C. Skamarock, 2000a: Long-lived mesoconvective vortices and their environment. Part II: Induced thermodynamic destabilization in idealized simulations. *Mon. Wea. Rev.*, **128**, 3396–3412.
- , —, and J. D. Tuttle, 2000b: Long-lived mesoconvective vortices and their environment. Part I: Observations from the central United States during the 1998 warm season. *Mon. Wea. Rev.*, **128**, 3376–3395.
- Zhang, D.-L., 1992: The formation of a cooling-induced mesovortex in the trailing stratiform region of a midlatitude squall line. *Mon. Wea. Rev.*, **120**, 2763–2785.
- , and J. M. Fritsch, 1987: Numerical simulation of the meso- β scale structure and evolution of the 1977 Johnstown flood. Part II: Inertially stable warm-core vortex and the mesoscale convective complex. *J. Atmos. Sci.*, **44**, 2593–2612.
- , and —, 1988: A numerical investigation of a convectively generated, inertially stable, extratropical warm-core mesovortex over land. Part I: Structure and evolution. *Mon. Wea. Rev.*, **116**, 2660–2687.
- , and N. Bao, 1996a: Oceanic cyclogenesis as induced by a mesoscale convective system moving offshore. Part I: A 90-h real-data simulation. *Mon. Wea. Rev.*, **124**, 1449–1469.
- , and —, 1996b: Oceanic cyclogenesis as induced by a mesoscale convective system moving offshore. Part II: Genesis and thermodynamic transformation. *Mon. Wea. Rev.*, **124**, 2206–2226.
- Zhang, F., 2005: Dynamics and structure of mesoscale error covariance of a winter cyclone estimated through short-range ensemble forecasts. *Mon. Wea. Rev.*, **133**, 2876–2893.
- , C. Snyder, and R. Rotunno, 2002: Mesoscale predictability of the “surprise” snowstorm of 24–25 January 2000. *Mon. Wea. Rev.*, **130**, 1617–1632.
- , —, and —, 2003: Effects of moist convection on mesoscale predictability. *J. Atmos. Sci.*, **60**, 1173–1185.
- , Z. Meng, and A. Aksoy, 2006a: Tests of an ensemble Kalman filter for mesoscale and regional-scale data assimilation. Part I: Perfect model experiments. *Mon. Wea. Rev.*, **134**, 722–736.
- , A. M. Odins, and J. W. Nielsen-Gammon, 2006b: Mesoscale predictability of an extreme warm-season precipitation event. *Wea. Forecasting*, **21**, 149–166.
- , N. Bei, R. Rotunno, C. Snyder, and C. C. Epifanio, 2007: Mesoscale predictability of moist baroclinic waves: Convection-permitting experiments and multistage error growth dynamics. *J. Atmos. Sci.*, in press.